JOURNAL OF MATERIALS SCIENCE 32 (1997) 5425–5437

A stress analysis model for composite coaxial cylinders

G. C. DAVIES, D. M. BRUCE
Silsoe Research Institute, Wrest Park, Silsoe, Bedfordshire, MK45 4HS, UK

An analytical model describing the elastic response of a system of coaxial thick-walled cylinders in contact is presented. The materials from which the cylinders are constructed must exhibit orthotropic elasticity. The loading can be uniaxial tension, torsion or internal pressure. The model allows inter- and intralaminar stresses to be determined. Examples of applications include pipes and light weight drive shafts reinforced with a helical winding, composite pressure vessels and single cells from fibrous plants such as flax and hemp.

Nomenclature

Symbol	Description
E_{11}, E_{22}, E_{33}	Young's moduli
G_{12}, G_{23}, G_{13}	Shear moduli
$\mu_{12}, \mu_{23}, \mu_{13}$	Poisson ratios
L_1, L_2, L_3, L_4	Differential operators
$\boldsymbol{M}$	Matrix used for solution of equations
$\boldsymbol{S}$	Compliance matrix
$\boldsymbol{T}$	Rotational transform matrix
T	Applied torque
s_{mn}	Element of $\boldsymbol{S}$
$M_{m,n}$	Element of $\boldsymbol{M}$
N	Number of layers of structure
P_{in}, P_{out}	Internal/external pressure
1, *2*, *3*	Orthogonal axes along material directions
r, θ, z	Orthogonal axes in cylindrical co-ordinates
σ_{rr} etc.	Normal stress
$\sigma_{r\theta}$ etc.	Shear stress
ε_{rr} etc.	Normal strain
$\varepsilon_{r\theta}$ etc.	Shear strain
u_r, u_θ, u_z	Displacements
β_{mn}	Reduced elastic coefficients
A, B, C, D, E, F	Constants to be determined
$\kappa, g_\kappa, \mu_1, \mu_2, h,$ H, η_m, δ_m	Elastic constants

1. Introduction

An advantage of using composite materials is that the materials as well as the structures can be designed to accommodate the applied load. Such design requires an understanding of the stress and of the resulting strains and displacements produced under loading. The simplest structures are axisymmetric shells with fibres wound in helices at angles of $\pm\theta$ to the axis of symmetry, which can be produced in an automatic process. High strength, low weight and corrosion resistance have led to the use of such components in many load bearing applications. Examples include aircraft and ship components, pressure vessels, reinforced piping and lightweight drive shafts.

The current study grew out of a model describing the states of stress and strain in a single plant fibre. There has recently been substantial interest in such fibres due to their attractive tensile properties (for example, the stiffness and strength of flax fibres are comparable to those of E-glass) and their renewability. Increased understanding of the mechanical behaviour of such fibres is necessary before they can be used with confidence as structural components. Structurally, these fibres can be considered as a number of thick-walled, concentric cylinders in contact. The model derived is therefore appropriate to both certain plant fibres and to more conventional engineering structures. Plant fibres are an order of magnitude stiffer and stronger than conventional thermoset and thermoplastic organic matrices, and have a similar cost [1]. This opens the possibility of reinforcing recycled matrix materials with plant fibres to regain strength lost during recycling. Plant fibres are safer to handle than glass fibres and can be disposed of at the end of their life cycle by burning. This is in contrast to glass fibres, which are generally disposed of as land-fill.

There has been a significant amount of work done on the elastic behaviour and failure of thin-walled filament-wound tubes. Spencer [2] described a method using axial and torsional vibration response for the measurement of axial and shear moduli of thin-walled shafts. Good agreement between theory and experiment was obtained, though dimensional and material data for the tubes used was not provided. Cazeneuve *et al.* [3] extended laminated plate theory to take account of the fact that filament winding in $\pm\theta$ crossed layers produces a fabric, rather than successive uni-directional layers crossed at angles $+\theta$ and $-\theta$. Introducing a gradual reduction of individual layer moduli in the orthotropic plate model permitted

0022–2461

the accurate prediction of the linear and non-linear response of thin-walled Kevlar/epoxy and carbon/epoxy $90/\pm\theta/90$ tubes. Soden *et al.* [4] presented an experimental study showing the effect of winding angle on the strength and deformation of reinforced tubes under internal pressure and axial loading. Filament-wound E-glass fibre reinforced epoxy-resin tubes of 100 mm diameter and 1 mm thickness were used. Stress–strain curves under three different types of loading demonstrated the effect of the winding angle on the elastic constants and on non-linear stress–strain behaviour. It was found that the magnitude of the elastic constants varied with winding angle as predicted by laminate theory.

Thick-walled filament wound pipes are readily available. Because the state of stress in these laminates under loading is three-dimensional, a three-dimensional stress–strain analysis is needed, which in turn requires three-dimensional mechanical properties. Al-Khalil and Soden [5] presented an analysis for determining theoretical values for the elastic constants needed for the three-dimensional stress analysis of angle-ply laminates, with an emphasis on filament-wound tubes. Effective elastic constants were calculated from the properties of uni-directional fibre-reinforced laminates for glass/epoxy, Kevlar/epoxy and carbon/epoxy composites.

Through-thickness stresses are particularly important as they can cause delamination. The stress distribution within a four-layer structure composed of fibre, coating, matrix and infinite surrounding composite received attention by Mikata and Taya [6]. The stresses in such a fibre when subjected to thermo–mechanical loading can cause cracking. Their model was later extended by Warwick and Clyne [7] to allow an outer layer of finite radius and generalized to any number of layers. Application of this model is limited to cases where the materials from which the coaxial components are made are isotropic in a plane normal to the cylinder axis.

Rosenow [8] obtained stress–strain responses for filament wound pipes constructed from polyester resin and glass fibres wound at six different winding angles. Biaxial loading, hoop pressure loading and tensile loading were used. Theoretical stress–strain responses, assuming that the radial stress was small and could be ignored, were compared to the experimental data. Agreement between theory and experiment was reasonable. The effect of including the radial stress in the calculations is investigated later in this paper.

2. The model

The theory presented here describes the stress analysis of structures composed of thick-walled concentric cylinders. Each cylindrical layer is made from an orthotropic material with a given filament winding angle, which can be different in each layer. An example structure is given in Fig. 1. Three layers are shown, but the analysis supports an arbitrary number. As with a model presented by Tang [9] describing the stress state in a single wood fibre, this model is based on theory by Lekhnitskii [10]. This theory describes the response of a homogeneous hollow cylinder having cylindrical anisotropy to an axially symmetric distribution of stress. The model here is an extension of [9] in that the effect of internal or external pressure (with ends capped or uncapped) and torsional loading can be included in addition to uniaxial loading. The torque required to prevent a helically reinforced structure from rotating can also be calculated. This may be significant in the case of helically wound plant fibres in a matrix in that the tendency for such fibres to rotate must be suppressed by interfacial shear stresses, which could contribute to fibre–matrix interfacial failure.

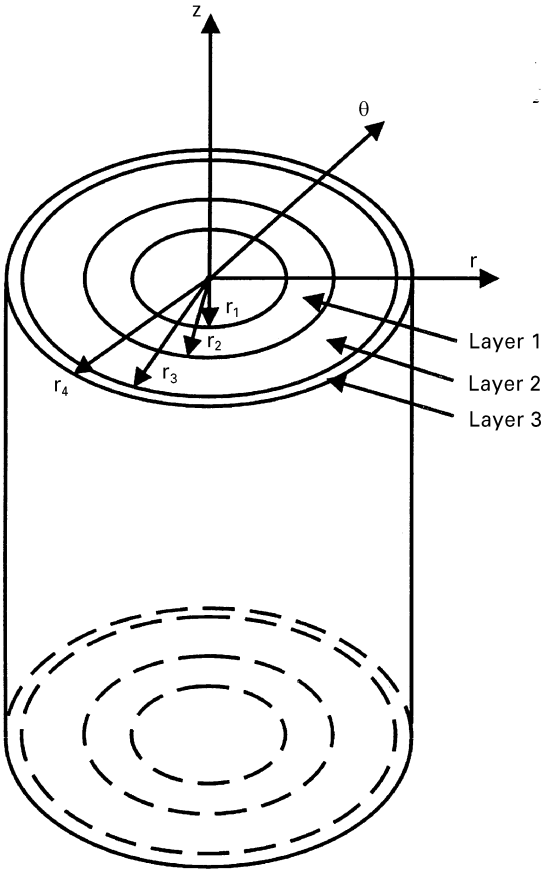

Figure 1 Example structure.

To perform the analysis, the elastic properties of the constituent composite layers must be determined. These may be already known, or samples of the material may be available for testing. If the properties of a material are difficult to obtain then it is possible to estimate them from the properties of its components. An example is a plant cell wall which has undergone secondary thickening, for simplicity considered to comprise cellulose fibres in a hemicellulose matrix. Values for the elastic properties of these components are available in the literature, so an estimate of the properties of the cell wall may be made.

Once the properties of the composite are determined for a given angle of fibre reinforcement, they can be calculated for any other angle using the tensor manipulation outlined in Appendix A. Thus, given the material properties of the components, a structure

comprising concentric cylinders each made from different materials and with different winding angles can be analysed.

The analysis is performed using linear elasticity theory and physically apparent boundary conditions of stress and displacement. A set of simultaneous equations is developed which can be solved using matrix methods outlined in Appendix B. Constants determined by the solution of these equations are then used to obtain explicit formulae for stress, strain and displacement.

3. Prediction of properties of the composite

There have been three different approaches adopted in estimating the properties of a composite material from the properties of its components. Bounding calculations have been used to establish, with varying degrees of complexity, upper and lower values of the elastic constants [11, 12]. Another method which can be used, with considerable computational demands, is finite element analysis [13]. Finally, analytical methods have been proposed which give exact solutions [14].

In this paper, the bounding method of Ward and Wilczynski [12] is used because it is computationally straightforward and gives quite close upper and lower bounds for all the elastic constants. These predictions were found to be close to those produced by more complex models. As with much other work [14, 15], Ward and Wilczynski's model requires that the fibres and matrix be either isotropic or transversely isotropic, leading to composite properties which are also transversely isotropic with respect to the material directions.

4. Examples

Three examples of the application of the theory are given below. At a glance it may seem that a glass fibre reinforced pipe (GRFP), a single plant fibre cell and a composite drive shaft have little in common. Each however has a structure which can be modelled with the theory given here.

4.1. GFRP tubes under biaxial pressure and axial loading

Experimental data from [8] is re-analysed here to determine the effect of including the radial stress in the calculations. In the absence of detailed specimen information from [8] the thickness of the anti-wicking barrier has been estimated from the area density of the mat used to construct it and the densities of its components. The structural layers have been assumed to be of equal thicknesses and arranged as in Table I. It is accepted that making such assumptions about the structure will affect the output from the model. However, the model is not especially sensitive to the detailed structure and so errors resulting from incorrect assumptions should be small.

The response to internal pressure of a GFRP pipe with a winding angle of 30°, is shown in Figs 2 and 3. Fig. 2 contains the original experimental data along with the results of the calculation by Rosenow and the results of this model. The convex shape of the experimental data is due to departures from linearity; it is not intended to model this effect. The theoretical lines should thus be compared to the initial part of the experimental curve which is approximately linear. Agreement of either theoretical line with the experimental data for small strains is reasonable. The model including the effect of radial stress predicts hoop strains of 8% less and axial strains of 28% greater than does the model due to Rosenow. The calculated variation of the hoop stress, axial stress, radial stress and hoop/axis shear stress through the wall thickness is shown in Fig. 3. Peak values of the radial and hoop stresses both occur at the inner surface. The peak value of the hoop stress in the inner load bearing layer

TABLE I GFRP data used in the model

Structure							
Layer	Inner radius (mm)	Outer radius (mm)	Area (%)	Winding angle (degrees)		Proportion fibre	Proportion matrix
Anti-wick layer	25.4	25.7	3.9	random		0.38	0.62
1	25.7	27.6	29.9	15, 30, 45, 60		0.38	0.62
2	27.6	29.5	32.0	−15, −30, −45, −60		0.38	0.62
3	29.5	31.4	34.2	15, 30, 45, 60		0.38	0.62
Properties of components							
	E_{33} (GPa)	E_{11} (GPa)	G_{13} (GPa)	G_{12} (GPa)	ν_{13}	ν_{12}	Reference
Glass fibre	77.2	77.2	30.9	30.9	0.25	0.25	[8]
Matrix	2.41	2.41	2.41	2.41	0.35	0.35	[8]
Properties of the composite along principal directions (average values calculated from Reference [12])							
Sheath	15.9	15.9	5.6	5.6	0.43	0.43	
Layers 1–3	30.8	7.3	3.1	3.1	0.31	0.2	

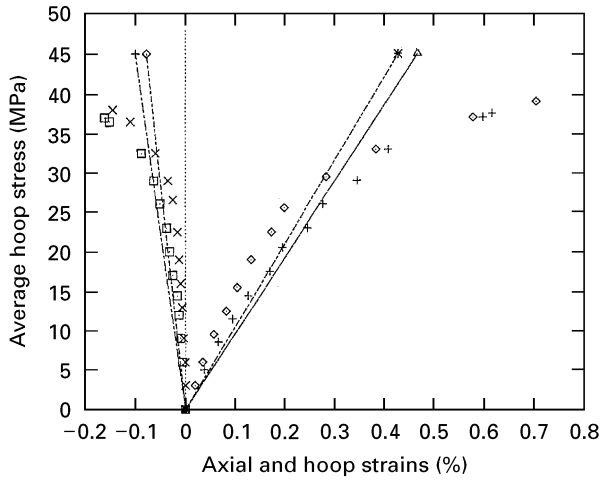

Figure 2 GFRP pipe (Table I) with a winding angle of 30° under internal pressure, producing biaxial loading. Comparison of theoretical models and experimental data. (◇) experimental hoop strain, test 1; (+) experimental hoop strain, test 2; (□) experimental axial strain, test 1; (×) experimental axial strain, test 2, (--△--) calculated hoop strain (Rosenow); (- ∗-) calculated hoop strain (this model); (--◇--) calculated axial strain (Rosenow) and (--+--) calculated axial strain (this model).

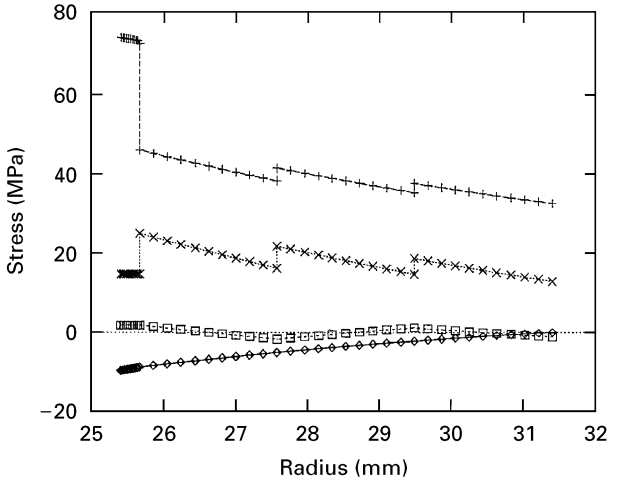

Figure 3 GFRP pipe (Table I) with a winding angle of 30° under internal pressure, producing biaxial loading. Predicted through-thickness stresses for an average hoop stress of 40 MPa. (—◇—) radial stress; (--+--) hoop stress; (--□--) hoop axial shear stress and (--×--) axial stress.

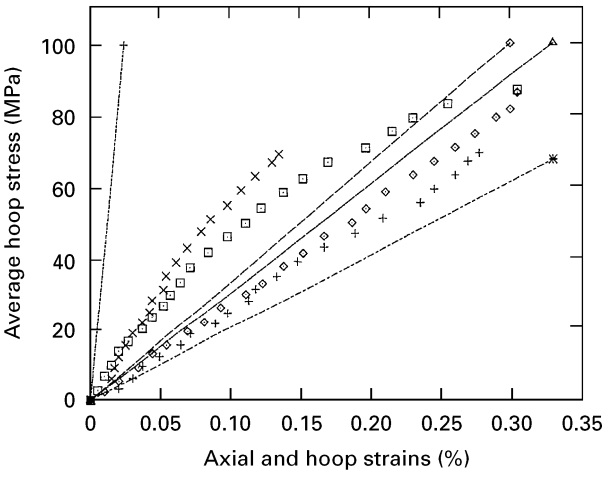

Figure 4 GFRP pipe (Table I) with a winding angle of 60° under internal pressure, producing biaxial loading. Comparison of theoretical models and experimental data. (◇) experimental hoop strain, test 1; (+) experimental hoop strain, test 2; (□) experimental axial strain, test 1; (×) experimental axial strain, test 2; (--△--) calculated hoop strain (Rosenow); (- ∗-) calculated hoop strain (this model); (--◇--) calculated axial strain (Rosenow) and (--+--) calculated axial strain (this model).

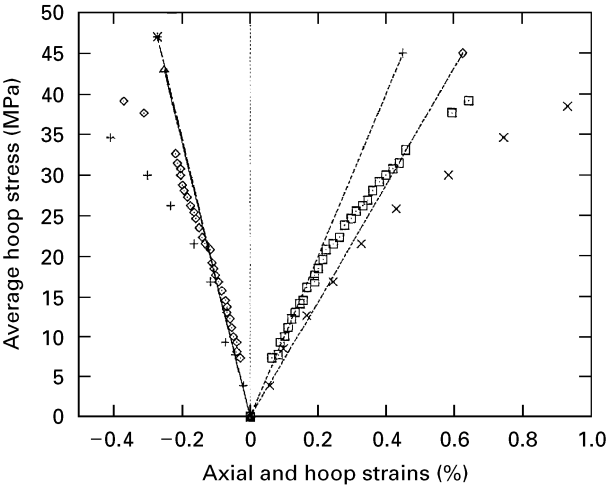

Figure 5 GFRP pipe (Table I) with a winding angle of 45° under uniaxial tension. Comparison of theoretical models and experimental data. (◇) experimental hoop strain, test 1; (+) experimental hoop strain, test 2; (□) experimental axial strain, test 1; (×) experimental axial strain, test 2; (--△--) calculated hoop strain (Rosenow); (--×--) calculated hoop strain (this model); (--◇--) calculated axial strain (Rosenow) and (--+--) calculated axial strain (this model).

(as opposed to the anti-wicking layer) is approximately five times that of the peak radial stress.

As the winding angle is altered, the behaviour of the tube changes. For a tube with a 60° winding angle under internal pressure, experimental data along with the theoretical prediction, due to Rosenow and of this model are given in Fig. 4. It is seen that the hoop and axial strains are both positive, though the predictions of the two models are significantly different. Rosenow's model predicts a smaller hoop strain and a substantially larger axial strain; it is this model which best fits the experimental data.

Fig. 5 shows the response of a GFRP pipe with a winding angle of 45° to uniaxial tension. The two theoretical lines agree well with the experimentally measured hoop strain and predict almost identical strains. However, the predicted axial strains are significantly different, with the new model predicting a strain of 28% less than that due to Rosenow's model. The experimental data (for small strains) lies between these two lines. Calculated stress variations through the thickness are shown in Fig. 6.

The behaviour under uniaxial tension of a GFRP pipe with a winding angle of 15° is given in Fig. 7. The model due to Rosenow fits the experimental data best, with the new model predicting significantly greater hoop and axial strains. The calculated variation of axial modulus with winding angle is shown in Fig. 8. This theory acceptably fits the limited data available from reference [8].

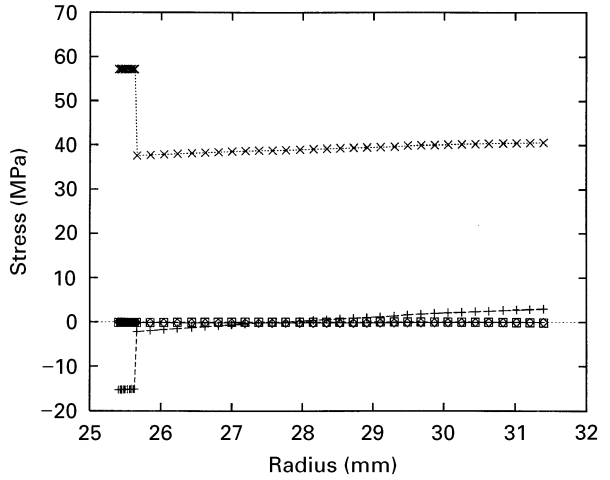

Figure 6 GFRP pipe (Table I) with a winding angle of 45° under uniaxial tension. Predicted through-thickness stresses for an average axial stress of 40 MPa. (◇) radial stress; (+) hoop stress; (□) hoop axial shear stress and (×) axial stress.

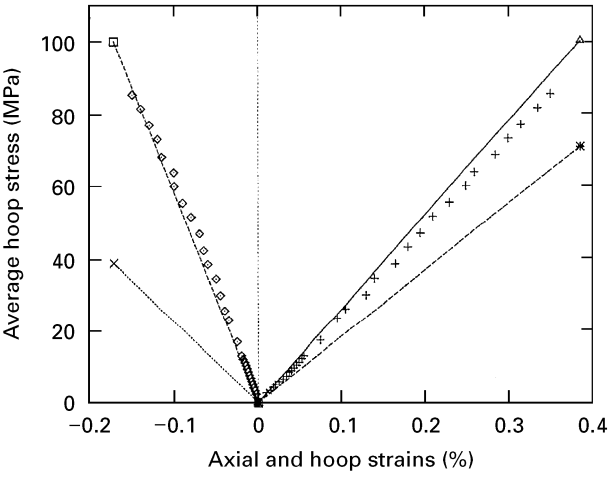

Figure 7 GFRP pipe (Table I) with a winding angle of 15° under uniaxial tension. Comparison of theoretical models and experimental data. (◇) experimental hoop strain; (+) experimental axial strain; (--⊡--) calculated hoop strain (Rosenow); (--×--) calculated hoop strain (this model); (--△--) calculated axial strain (Rosenow) and (- ∗-) calculated axial strain (this model).

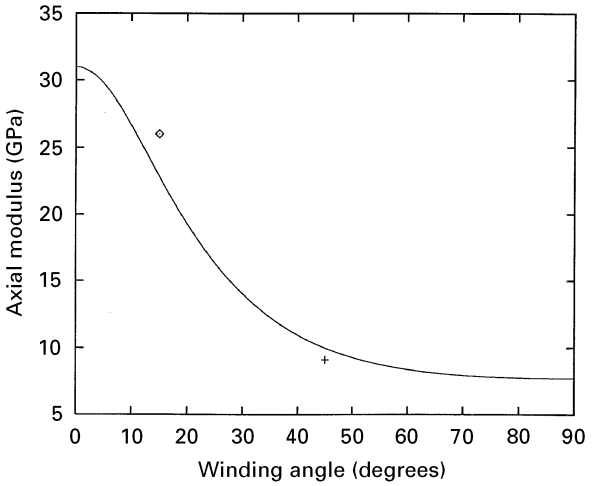

Figure 8 Variation in axial modulus with winding angle for GFRP pipe (Table I). (–) calculated modulus; (◇) 15° pipe and (+) 45° pipe.

4.2. Application to single flax fibre cells

There is substantial interest in the engineering properties of fibrous crops such as flax and hemp. The renewability of naturally occurring fibres is clearly an attraction, but their variability can cause problems in maintaining consistent mechanical properties of structures. A greater understanding of these mechanical properties is required before they can be properly designed. Properties of single flax fibre cells are given in Table II.

Single flax fibres are typically between 25–30 mm long and 14–30 μm in diameter [16]. The cell wall mainly comprises cellulose and hemicellulose, with small quantities of pectin and lignin. The cellulose and hemicellulose combine in the cell wall to form a microfibrilar structure. Within the cell wall the microfibrils are arranged in layers (lamellae). The angles of the microfibrils to the axis of the cell are different in each lamella. There are three such layers, known as S1, S2 and S3, surrounding a hollow lumen. All these layers have undergone the process of secondary-thickening, with the S2 layer being structurally dominant. The

TABLE II Flax data used in the model

Structure							
Layer	Inner radius (μm)	Outer radius (μm)	Area (%)	Winding angle (degrees)		Proportion fibre	Proportion matrix
S1	3.2	4.5	10	– 30		0.793	0.207
S2	4.5	9.5	80	6.5		0.793	0.207
S3	9.5	1.0	10	– 30		0.793	0.207
Properties of components							
	E_{33} (MPa)	E_{11} (MPa)	G_{13} (MPa)	G_{12} (MPa)	ν_{13}	ν_{12}	Reference
Cellulose	134	27.2	6.60	4.40	0.1	0.04	[18]
Hemicellulose	2	–	0.769	–	0.3	–	[18]
Properties of the composite along principal directions (average values calculated from Reference [12])							
Cell wall (all layers)	81.2	7.77	2.17	3.49	0.022	0.113	

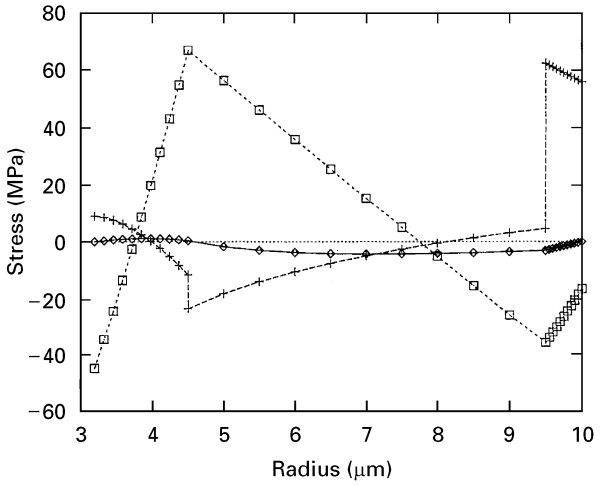

Figure 9 Single flax fibre under an applied axial stress of 1 GPa (Table II). Predicted through-thickness (◇) radial, (+) hoop and (□) hoop–axial shear stresses.

winding angle in the S1 and S3 layers is in the same sense and is taken to be at an angle of 30° to the fibre axis. The angle in the S2 layer is in the opposite sense and is typically around 6.5° [17]. For the sake of simplicity and in the absence of more accurate data, it is assumed that all three layers are compositionally identical.

The variation of the calculated radial, hoop and hoop-axial shear stresses through the wall thickness of a single fibre cell under a uniaxial stress of 1 GPa is shown in Fig. 9. The peak value of the shear stress occurs between the S1 and S2 layers and is 6.7% of the average axial stress. The peak value of the hoop stress occurs between the S2 and S3 layers and is 6.3% of the average axial stress. The radial stress is smaller and peaks at 0.4% of the axial stress within the S2 layer.

4.3. Composite tubes to transmit torque

Driveshafts made from composite materials have some significant advantages over those made from metals. They exhibit a higher specific stiffness, allowing components to be lighter and increasing the critical speed for whirling. This in turn reduces the number of bearings necessary [19], thus reducing fuel consumption. At the manufacturing stage, fine tuning of the driveshaft properties is possible in a manner which is not possible using isotropic materials such as metals. For example, use of composite shafts allows the torsional spring rate to be altered independently of the diameter of the shaft. Properties of an example shaft are given in Table III.

The structure of the shaft will affect both its stiffness (torsional and axial) and the stress distribution within it. The variation of radial, hoop and hoop-axial shear stresses through the wall thickness due to an imposed axial torque of 1000 Nm for a winding angle of 45° is given in Fig. 1a. The calculated variation of torsional stiffness with winding angle is given in Fig. 11.

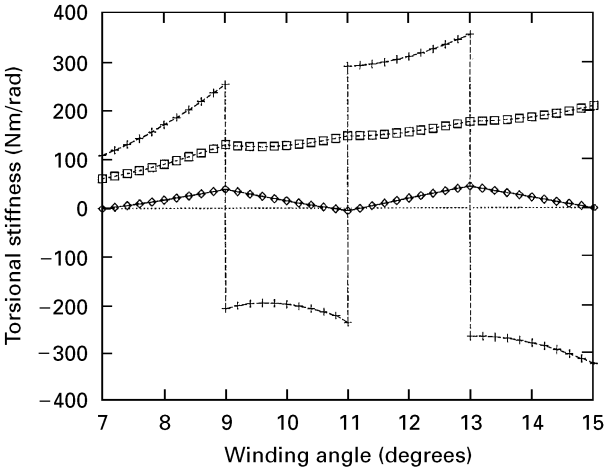

Figure 10 Response of CFRP shaft (Table III) to an applied torque of 1000 Nm. (◇) Radial, (+) hoop and (□) hoop–axial shear stress as a function of radius for a winding angle of 45°.

TABLE III CFRP tube data used in the model

Structure

Layer	Inner radius (mm)	Outer radius (mm)	Area (%)	Winding angle (degrees)	Proportion fibres	Proportion matrix
1	7.00	9.00	18.2	+ 45	0.4	0.6
2	9.00	11.0	22.7	− 45	0.4	0.6
3	11.0	13.0	27.3	+ 45	0.4	0.6
4	13.0	15.0	31.8	− 45	0.4	0.6

Properties of components

	E_{33} (GPa)	E_{11} (GPa)	G_{13} (GPa)	G_{12} (MPa)	ν_{13}	ν_{12}	Reference
Carbon fibre	300.0	300.0	115.4	115.4	0.3	0.3	[20, p. 31]
Epoxy	4.00	–	1.48	–	0.35	–	[20, p. 6]

Properties of the composite along principal directions (average values calculated from Reference [12])

Composite layers	181.6	23.2	5.71	10.34	0.313	0.1242

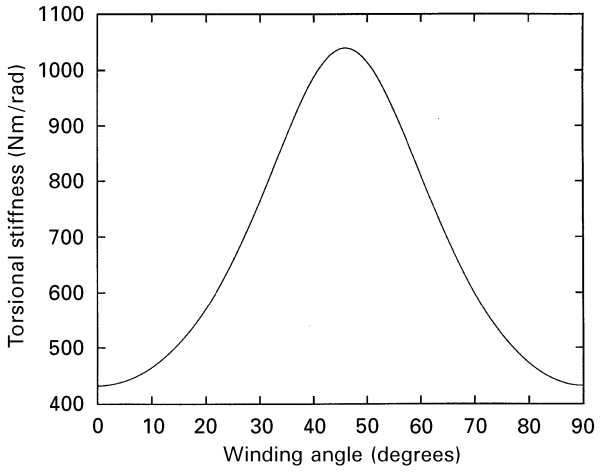

Figure 11 Calculated torsional stiffness of CFRP shaft (Table III) as a function of the fibre winding angle.

5. Conclusions

An analysis of the elastic response of a system of thick-walled, concentric coaxial cylinders has been presented. Including the radial stress in the analysis adds significantly to the complexity of the model. Using the model to re-analyse previously obtained data on the behaviour of glass fibre reinforced pipes under biaxial and uniaxial loading indicates a variable fit with experimental data and a previous model. This suggests that the influence of the radial stress should not always be ignored. The stress variations through the wall thickness of thick-walled cylinders are significant and the peak stress can be significantly greater than the mean stress. This has implications for the criteria used to design such structures.

Appendix A. Elastic constants and rotation

A.1. The compliance matrix for an orthotropic material

In three dimensions for an elastic body with orthotropic symmetry there are nine independent elastic coefficients. The compliance matrix referred to the axes of symmetry is given by [21]:

$$\boldsymbol{S} = \begin{bmatrix} \frac{1}{E_{11}} & -\frac{\nu_{21}}{E_{22}} & -\frac{\nu_{31}}{E_{33}} & 0 & 0 & 0 \\ -\frac{\nu_{12}}{E_{11}} & \frac{1}{E_{22}} & -\frac{\nu_{32}}{E_{33}} & 0 & 0 & 0 \\ -\frac{\nu_{13}}{E_{11}} & -\frac{\nu_{23}}{E_{22}} & \frac{1}{E_{33}} & 0 & 0 & 0 \\ 0 & 0 & 0 & \frac{1}{G_{23}} & 0 & 0 \\ 0 & 0 & 0 & 0 & \frac{1}{G_{13}} & 0 \\ 0 & 0 & 0 & 0 & 0 & \frac{1}{G_{12}} \end{bmatrix} \quad \text{(A1)}$$

A.2. Off-axis loading of a unidirectional composite

Composite materials are not always conveniently arranged with the fibre axis co-linear with the direction of loading. Such an arrangement gives good tensile properties along the fibre direction but poor stiffness and strength perpendicular to this. Thus in practice, both in natural and man-made structures, the fibres are arranged such that the loading is off-axis. It is useful to define a compliance matrix for an arbitrary angle of rotation between the direction of loading and the fibre axis.

Consider a state of stress σ referred to a set of axes (r, θ, z). This can be represented in an alternative (orthogonal) set of axes $(1, 2, 3)$ through multiplication by the transformation matrix $\boldsymbol{T}$:

$$\sigma_{123} = \boldsymbol{T}\sigma_{r\theta z} \quad \text{(A2)}$$

A similar transformation is used to transform strain between axes. In this case:

$$\bar{\varepsilon}_{123} = \boldsymbol{T}\bar{\varepsilon}_{r\theta z} \quad \text{(A3)}$$

The terms ε_{123} are related to $\bar{\varepsilon}_{123}$ by:

$$\varepsilon_{123} = \boldsymbol{R}\,.\,\bar{\varepsilon}_{123} \quad \text{(A4)}$$

where

$$\boldsymbol{R} = \begin{bmatrix} 1 & 0 & 0 & 0 & 0 & 0 \\ 0 & 1 & 0 & 0 & 0 & 0 \\ 0 & 0 & 1 & 0 & 0 & 0 \\ 0 & 0 & 0 & 2 & 0 & 0 \\ 0 & 0 & 0 & 0 & 2 & 0 \\ 0 & 0 & 0 & 0 & 0 & 2 \end{bmatrix} \quad \text{(A5)}$$

The stresses and strains written out in full are:

$$\sigma_{123} = \{\sigma_{11}\ \sigma_{22}\ \sigma_{33}\ \sigma_{23}\ \sigma_{13}\ \sigma_{12}\} \quad \text{(A6)}$$

$$\sigma_{r\theta z} = \{\sigma_r\ \sigma_\theta\ \sigma_r\ \sigma_{\theta z}\ \sigma_{rz}\ \sigma_{r\theta}\} \quad \text{(A7)}$$

$$\bar{\varepsilon}_{123} = \{\varepsilon_{11}\ \varepsilon_{22}\ \varepsilon_{33}\ \tfrac{1}{2}\varepsilon_{23}\ \tfrac{1}{2}\varepsilon_{13}\ \tfrac{1}{2}\varepsilon_{12}\} \quad \text{(A8)}$$

$$\bar{\varepsilon}_{r\theta z} = \{\varepsilon_r\ \varepsilon_\theta\ \varepsilon_z\ \tfrac{1}{2}\varepsilon_{\theta z}\ \tfrac{1}{2}\varepsilon_{rz}\ \tfrac{1}{2}\varepsilon_{r\theta}\} \quad \text{(A9)}$$

For a rotation about the r axis by an angle α, equation (A2) becomes:

$$\begin{bmatrix} \sigma_{11} \\ \sigma_{22} \\ \sigma_{33} \\ \sigma_{23} \\ \sigma_{13} \\ \sigma_{12} \end{bmatrix} = \begin{bmatrix} 1 & 0 & 0 & 0 & 0 & 0 \\ 0 & \cos^2(\alpha) & \sin^2(\alpha) & \cos(\alpha)\sin(\alpha) & 0 & 0 \\ 0 & \sin^2(\alpha) & \cos^2(\alpha) & -\cos(\alpha)\sin(\alpha) & 0 & 0 \\ 0 & -\cos(\alpha)\sin(\alpha) & \cos(\alpha)\sin(\alpha) & \cos^2(\alpha) - \sin^2(\alpha) & 0 & 0 \\ 0 & 0 & 0 & 0 & \cos(\alpha) & -\sin(\alpha) \\ 0 & 0 & 0 & 0 & \sin(\alpha) & \cos(\alpha) \end{bmatrix} \cdot \begin{bmatrix} \sigma_r \\ \sigma_\theta \\ \sigma_z \\ \sigma_{\theta z} \\ \sigma_{rz} \\ \sigma_{r\theta} \end{bmatrix} \quad \text{(A10)}$$

A.3. Transformation of the compliance matrix

Define a compliance matrix $\boldsymbol{S}$ relating strain to stress in the $(1,2,3)$ axes such that:

$$\varepsilon_{123} = \boldsymbol{S}\sigma_{123} \tag{A11}$$

substituting for σ_{123} from Equation (A2):

$$\varepsilon_{123} = \boldsymbol{ST}\sigma_{r\theta z} \tag{A12}$$

premultiplying both sides of Equation (A3) with $\boldsymbol{T}^{-1}$ and substituting $\bar{\varepsilon}_{123}$ from Equation (A4) gives:

$$\bar{\varepsilon}_{r\theta z} = \boldsymbol{T}^{-1}\boldsymbol{R}^{-1}\varepsilon_{123} \tag{A13}$$

The strain in (r,θ,z) co-ordinates is therefore

$$\begin{aligned}\varepsilon_{r\theta z} &= \boldsymbol{RT}^{-1}\boldsymbol{R}^{-1}\boldsymbol{ST}\sigma_{r\theta z} \\ &= \boldsymbol{S}^{*}\sigma_{r\theta z}\end{aligned} \tag{A14}$$

Thus the compliance matrix for the new set of axes is determined.

Appendix B. Elastic solution

B.1. General theory

The governing partial differential equations of a hollow cylinder with body forces absent are given as [10, p. 129]

$$L_4'\phi + L_3'\psi = 0 \tag{A15}$$

$$L_3''\phi + L_2'\psi = \frac{Fs_{34}}{r} - 2D \tag{A16}$$

ϕ and ψ are stress functions, F is a constant, D the relative angle of twist, s_{34} an elastic constant and L_4', L_3', L_3'' and L_2' are differential operators defined by:

$$\begin{aligned}L_2' = {} & \beta_{44}\frac{\partial^2}{\partial r^2} - 2\beta_{45}\frac{1}{r}\frac{\partial^2}{\partial r\partial\theta^2} + \beta_{55}\frac{1}{r^2}\frac{\partial^2}{\partial\theta^2} \\ & + \beta_{44}\frac{1}{r}\frac{\partial}{\partial r}\end{aligned} \tag{A17}$$

$$\begin{aligned}L_3' = {} & -\beta_{24}\frac{\partial^3}{\partial r^3} + (\beta_{25}+\beta_{46})\frac{1}{r}\frac{\partial^3}{\partial r^2\partial\theta} \\ & - (\beta_{14}+\beta_{56})\frac{1}{r^2}\frac{\partial^3}{\partial r\partial\theta^2} + \beta_{15}\frac{1}{r^3}\frac{\partial^3}{\partial\theta^3} \\ & + (\beta_{14}-2\beta_{44})\frac{1}{r}\frac{\partial^2}{\partial r^2} + (\beta_{46}-2\beta_{15}) \\ & \times\frac{1}{r^2}\frac{\partial^2}{\partial r\partial\theta} + \beta_{15}\frac{1}{r^2}\frac{\partial}{\partial\theta}\end{aligned} \tag{A18}$$

$$\begin{aligned}L_3'' = {} & -\beta_{24}\frac{\partial^3}{\partial r^3} + (\beta_{25}+\beta_{46})\frac{1}{r}\frac{\partial^3}{\partial r^2\partial\theta} \\ & - (\beta_{14}+\beta_{56})\frac{1}{r^2}\frac{\partial^3}{\partial r\partial\theta^2} + \beta_{15}\frac{1}{r^3}\frac{\partial^3}{\partial\theta^3} \\ & - (\beta_{14}+\beta_{24})\frac{1}{r}\frac{\partial^2}{\partial r^2} + (\beta_{15}-2\beta_{46})\frac{1}{r^2}\frac{\partial^2}{\partial r\partial\theta} \\ & + (\beta_{14}+\beta_{56})\frac{1}{r^3}\frac{\partial^2}{\partial\theta^2} + \beta_{46}\frac{1}{r^3}\frac{\partial}{\partial\theta}\end{aligned} \tag{A19}$$

$$\begin{aligned}L_4' = {} & \beta_{22}\frac{\partial^4}{\partial r^4} - 2\beta_{26}\frac{1}{r}\frac{\partial^4}{\partial r^3\partial\theta} + (2\beta_{12}+\beta_{66})\frac{1}{r^2}\frac{\partial^4}{\partial r^2\partial\theta^2} \\ & - 2\beta_{16}\frac{1}{r^3}\frac{\partial^4}{\partial r\partial\theta^3} + \beta_{11}\frac{1}{r^4}\frac{\partial^4}{\partial\theta^4} + 2\beta_{22}\frac{1}{r}\frac{\partial^3}{\partial r^3} \\ & - (2\beta_{12}+\beta_{66})\frac{1}{r^3}\frac{\partial^3}{\partial r\partial\theta^2} + 2\beta_{16}\frac{1}{r^4}\frac{\partial^3}{\partial\theta^3} \\ & - \beta_{11}\frac{1}{r^2}\frac{\partial^2}{\partial r^2} - 2(2\beta_{16}+\beta_{26})\frac{1}{r^3}\frac{\partial^2}{\partial r\partial\theta} \\ & + (2\beta_{11}+2\beta_{12}+\beta_{66})\frac{1}{r^4}\frac{\partial^2}{\partial\theta^2} + \beta_{11}\frac{1}{r^3}\frac{\partial}{\partial r} \\ & + (2\beta_{16}+\beta_{26})\frac{1}{r^4}\frac{\partial}{\partial\theta}\end{aligned} \tag{A20}$$

where β_{mn} are the reduced elastic coefficients defined in Equation (A33).

The stress distribution in a hollow cylinder subjected to symmetrical loading is symmetrical about the axis, hence the stress functions ϕ and ψ will only depend on the radius r. The system of equations for ϕ and ψ becomes [10, p. 232]

$$\begin{aligned}& \beta_{22}\left(\phi'''' + \frac{2\phi'''}{r}\right) + \beta_{11}\left(-\frac{\phi''}{r^2} + \frac{\phi'}{r^3}\right) - \beta_{24}\psi''' \\ & + (\beta_{14}-2\beta_{24})\frac{\psi''}{r} = 0\end{aligned} \tag{A21}$$

$$\begin{aligned}& -\beta_{24}\phi''' - (\beta_{14}+\beta_{24})\frac{\phi''}{r} + \beta_{44}\left(\psi'' + \frac{\psi'}{r}\right) \\ & = \frac{Fs_{34}}{r} - 2D\end{aligned} \tag{A22}$$

The general solution of Equations (A21 and A22) is:

$$\begin{aligned}\phi = {} & E\frac{\beta_{14}}{\beta_{11}}r + \frac{A}{2}r^2 + \frac{B}{1+\kappa}r^{1+\kappa} + \frac{C}{1-\kappa}r^{1-\kappa} \\ & + H + \frac{D\mu_1}{3}r^3\end{aligned} \tag{A23}$$

$$\begin{aligned}\psi = {} & E\ln r + A\frac{s_{34}}{\beta_{44}}r + Ag_1 r + \frac{B}{\kappa}g_\kappa r^\kappa \\ & - \frac{C}{\kappa}g_{-\kappa}r^{-\kappa} + H - \frac{D\mu_2}{2}r^2\end{aligned} \tag{A24}$$

where A, B etc. are constants to be found. In determining displacements and requiring that they be a single-valued function of the co-ordinates, it is necessary that [10]

$$E = 0 \tag{A25}$$

$$A = Fh \tag{A26}$$

In a cylindrical co-ordinate system with an axially symmetric stress distribution, the stress functions are related to the stress components by [10, p. 128]:

$$\sigma_{rr} = \frac{\phi'(r)}{r} \tag{A27}$$

$$\sigma_{\theta\theta} = \phi''(r) \tag{A28}$$

$$\sigma_{\theta z} = \psi'(r) \tag{A29}$$

$$\sigma_{zz} = F - \frac{1}{s_{33}}\left(s_{13}\sigma_{rr} + s_{23}\sigma_{\theta\theta} + s_{34}\sigma_{\theta z}\right) \tag{A30}$$

$$\sigma_{r\theta} = 0 \tag{A31}$$

$$\sigma_{rz} = 0 \tag{A32}$$

B.2. Elastic constants

It is convenient to define a number of elastic constants for use in the analysis. The reduced elastic constants in the jth layer are defined as

$$\beta_{mn}^{(j)} = \left[s_{mn}^{(j)} - \frac{s_{m3}^{(j)} s_{n3}^{(j)}}{s_{33}} \right] \tag{A33}$$

where $m,\ n = 1, 2, 4, 5, 6$. Other constants in the jth layer are:

$$\kappa_j = \left(\frac{\beta_{11}^{(j)}\beta_{44}^{(j)} - \beta_{14}^{(j)^2}}{\beta_{22}^{(j)}\beta_{44}^{(j)} - \beta_{24}^{(j)^2}} \right)^{\frac{1}{2}} \tag{A34}$$

$$g_{\kappa_j}^{(j)} = \frac{\beta_{14}^{(j)} + \kappa_j \beta_{24}^{(j)}}{\beta_{44}^{(j)}} \tag{A35}$$

$$\mu_1^{(j)} = \frac{\beta_{14}^{(j)} - 2\beta_{24}^{(j)}}{4(\beta_{22}^{(j)}\beta_{44}^{(j)} - \beta_{24}^{(j)^2}) - (\beta_{11}^{(j)}\beta_{44}^{(j)} - \beta_{14}^{(j)^2})} \tag{A36}$$

$$\mu_2^{(j)} = -\frac{\beta_{11}^{(j)} - 4\beta_{22}^{(j)}}{4(\beta_{22}^{(j)}\beta_{44}^{(j)} - \beta_{24}^{(j)^2}) - (\beta_{11}^{(j)}\beta_{44}^{(j)} - \beta_{14}^{(j)^2})} \tag{A37}$$

$$h^{(j)} = \frac{(s_{13}^{(j)} - s_{23}^{(j)})\beta_{44}^{(j)} - s_{34}^{(j)}(\beta_{14}^{(j)} - \beta_{24}^{(j)})}{(\beta_{22}^{(j)}\beta_{44}^{(j)} - \beta_{24}^{(j)^2}) - (\beta_{11}^{(j)}\beta_{44}^{(j)} - \beta_{14}^{(j)^2})} \tag{A38}$$

$$\delta_1^{(j)} = 1 - \frac{1}{s_{33}^{(j)}}\left(s_{13}^{(j)} + s_{23}^{(j)} - s_{34}^{(j)} g_1^{(j)}\right) h^{(j)} + \frac{s_{34}^{(j)^2}}{s_{33}^{(j)}\beta_{44}^{(j)}} \tag{A39}$$

$$\delta_2^{(j)} = \frac{-s_{13}^{(j)} - s_{23}^{(j)}\kappa_j + s_{34}^{(j)} g_{-\kappa_j}}{s_{33}^{(j)}} \tag{A40}$$

$$\delta_3^{(j)} = \frac{-s_{13}^{(j)} + s_{23}^{(j)}\kappa_j + s_{34}^{(j)} g_{-\kappa_j}}{s_{33}^{(j)}} \tag{A41}$$

$$\delta_4^{(j)} = \frac{-(s_{13}^{(j)} + 2s_{23}^{(j)})\mu_1^{(j)} - s_{34}^{(j)}\mu_2^{(j)}}{s_{33}^{(j)}} \tag{A42}$$

$$[\eta_1^{(j)}]_i = (\beta_{m1}^{(j)} + \beta_{m2}^{(j)} - \beta_{m4}^{(j)} g_{\kappa_1}^{(1)}) h^{(j)} + s_{m3}^{(j)} - \beta_{m4}^{(j)} \frac{s_{34}^{(j)}}{\beta_{44}^{(j)}} \tag{A43}$$

$$[\eta_2^{(j)}]_i = \beta_{m1}^{(j)} + \beta_{m2}^{(j)}\kappa_j - \beta_{m4}^{(j)} g_{\kappa_j}^{(j)} \tag{A44}$$

$$[\eta_3^{(j)}]_i = \beta_{m1}^{(j)} - \beta_{m2}^{(j)}\kappa_j - \beta_{m4}^{(j)} g_{-\kappa_j}^{(j)} \tag{A45}$$

$$[\eta_4^{(j)}]_i = (\beta_{m1}^{(j)} + 2\beta_{m2}^{(j)})\mu_1^{(j)} + \beta_{m4}^{(j)}\mu_2^{(j)} \tag{A46}$$

where $i = 1 \ldots 4$.

B.3. Solution for stresses

The stresses in the jth layer are obtained from Equations (A27–32)

$$\sigma_{rr}^{(j)} = F^{(j)}h^{(j)} + B^{(j)} r^{\kappa_j - 1} + C^{(j)} r^{-\kappa_j - 1} + D^{(j)}\mu_1^{(j)} r \tag{A47}$$

$$\sigma_{\theta\theta}^{(j)} = F^{(j)}h^{(j)} + B^{(j)}\kappa_j r^{\kappa_j - 1} - C^{(j)}\kappa_j r^{-\kappa_j - 1} + 2D^{(j)}\mu_1^{(j)} r \tag{A48}$$

$$\sigma_{\theta z}^{(j)} = -F^{(j)}\frac{s_{34}^{(j)}}{\beta_{44}^{(j)}} - F^{(j)}h^{(j)}g_1^{(j)} - B^{(j)}g_{\kappa_j}^{(j)} r^{\kappa_j - 1} - C^{(j)}g_{-\kappa_j}^{(j)} r^{-\kappa_j - 1} + D^{(j)}\mu_2^{(j)} r \tag{A49}$$

$$\sigma_{zz}^{(j)} = F^{(j)}\delta_1^{(j)} + B^{(j)}\delta_2^{(j)} r^{\kappa_j - 1} + C^{(j)}\delta_3^{(j)} r^{-\kappa_j - 1} + D^{(j)}\delta_4^{(j)} r \tag{A50}$$

$$\sigma_{r\theta}^{(j)} = 0 \tag{A51}$$

$$\sigma_{rz}^{(j)} = 0 \tag{A52}$$

The superscripts or subscripts j indicate the particular layers. $A^{(j)}$, $B^{(j)}$, etc. are constants to be determined from the boundary conditions.

B.4. Solution for strains

Strains are related to stresses by Equations (A15 and A16). Substituting for stresses from Equations (A47–A52) and using the constants in section (B.2) the strains are obtained as:

$$\varepsilon_{rr}^{(j)} = B^{(j)}[\eta_2^{(j)}]_1 r^{\kappa_j - 1} + C^{(j)}[\eta_3^{(j)}]_1 r^{-\kappa_j - 1} + D^{(j)}[\eta_4^{(j)}]_1 r + F^{(j)}[\eta_1^{(j)}]_1 \tag{A53}$$

$$\varepsilon_{\theta\theta}^{(j)} = B^{(j)}[\eta_2^{(j)}]_2 r^{\kappa_j - 1} + C^{(j)}[\eta_3^{(j)}]_2 r^{-\kappa_j - 1} + D^{(j)}[\eta_4^{(j)}]_2 r + F^{(j)}[\eta_1^{(j)}]_2 \tag{A54}$$

$$\varepsilon_{zz}^{(j)} = B^{(j)}[\eta_2^{(j)}]_3 r^{\kappa_j - 1} + C^{(j)}[\eta_3^{(j)}]_3 r^{-\kappa_j - 1} + D^{(j)}[\eta_4^{(j)}]_3 r + F^{(j)}[\eta_1^{(j)}]_3 \quad \text{(A55)}$$

$$\varepsilon_{\theta z}^{(j)} = B^{(j)}[\eta_2^{(j)}]_4 r^{\kappa_j - 1} + C^{(j)}[\eta_3^{(j)}]_4 r^{-\kappa_j - 1} + D^{(j)}[\eta_4^{(j)}]_4 r + F^{(j)}[\eta_1^{(j)}]_4 \quad \text{(A56)}$$

$$\varepsilon_{rz}^{(j)} = 0 \quad \text{(A57)}$$

$$\varepsilon_{r\theta}^{(j)} = 0 \quad \text{(A58)}$$

B.5. Radial and axial displacements

In cylindrical co-ordinates, displacement in the jth layer is related to strain by [22, p. 342]:

$$\varepsilon_{rr}^{(j)} = \frac{\partial u_r^{(j)}}{\partial r} \quad \text{(A59)}$$

$$\varepsilon_{\theta\theta}^{(j)} = \frac{1}{r}\frac{\partial u_\theta^{(j)}}{\partial \theta} + \frac{u_r^{(j)}}{r} \quad \text{(A60)}$$

$$\varepsilon_{zz}^{(j)} = \frac{\partial u_z^{(j)}}{\partial z} \quad \text{(A61)}$$

$$\varepsilon_{\theta z}^{(j)} = \frac{\partial u_\theta^{(j)}}{\partial z} + \frac{1}{r}\frac{\partial u_z^{(j)}}{\partial \theta} \quad \text{(A62)}$$

$$\varepsilon_{rz}^{(j)} = \frac{\partial u_z^{(j)}}{\partial r} + \frac{\partial u_r^{(j)}}{\partial z} \quad \text{(A63)}$$

$$\varepsilon_{r\theta}^{(j)} = \frac{1}{2}\left(\frac{1}{r}\frac{\partial u_r^{(j)}}{\partial \theta} + \frac{\partial u_\theta^{(j)}}{\partial r} - \frac{u_\theta^{(j)}}{r}\right) \quad \text{(A64)}$$

In the case of a symmetrical stress distribution, the terms which depend on θ are zero. From Equation (A60) the radial displacement in layer j can be expressed as:

$$u_r^{(j)} = r\varepsilon_{\theta\theta}^{(j)}$$

Substituting for $\varepsilon_{\theta\theta}$ from Equation (A54) gives the final expression for u_r:

$$u_r^{(j)} = B^{(j)}[\eta_2^{(j)}]_2 r^{\kappa_j} + C^{(j)}[\eta_3^{(j)}]_2 r^{-\kappa_j} + D^{(j)}[\eta_4^{(j)}]_2 r^2 + F^{(j)}[\eta_1^{(j)}]_2 r \quad \text{(A65)}$$

From Equation (A61) the axial displacement can be expressed as:

$$u_z^{(j)} = \int \varepsilon_{zz}^{(j)}\,dz$$

Substituting for ε_{zz} taking $u_z = 0$ at $z = 0$ from Equation (A55) gives:

$$u_z^{(j)} = (B^{(j)}[\eta_2^{(j)}]_3 r^{\kappa_j - 1} + C^{(j)}[\eta_3^{(j)}]_3 r^{-\kappa_j - 1} + D^{(j)}[\eta_4^{(j)}]_3 r + F^{(j)}[\eta_1^{(j)}]_3)z \quad \text{(A66)}$$

B.6. Boundary conditions

The boundary conditions for the radial and tangential stress at the inner surfaces are:

$$\sigma_{rr}^{(1)} = -P_{in} \quad \text{(A67)}$$

$$\sigma_{rr}^{(N)} = -P_{out} \quad \text{(A68)}$$

At the contact surfaces of adjacent layers, the following stress and displacement relationships must hold

$$\sigma_{rr}^{(j)} = \sigma_{rr}^{(j+1)} \quad \text{(A69)}$$

$$u_r^{(j)} = u_r^{(j+1)} \quad \text{(A70)}$$

$$\sigma_{\theta z}^{(j)} = \sigma_{\theta z}^{(j+1)} \quad \text{(A71)}$$

$$u_z^{(j)} = u_z^{(j+1)} \quad \text{(A72)}$$

Integrating the axial stress across the section gives the applied axial load:

$$\sum_{n=1}^{N} \int_{r_n}^{r_{n+1}} \sigma_{zz}^{(n)} r\,dr = \frac{P}{2\pi} \quad \text{(A73)}$$

The shear stress in the fibre is related to the applied moment by:

$$\sum_{n=1}^{N} \int_{r_n}^{r_{n+1}} \sigma_{\theta z}^{(n)} r^2\,dr = \frac{T}{2\pi} \quad \text{(A74)}$$

B.7. Construction of the matrix

Using the boundary conditions of Equations (A67–A74) leads to a set of simultaneous equations best solved by matrix algebra.

A matrix $\boldsymbol{M}$ is defined such that

$$M \cdot \begin{pmatrix} B^{(1)} \\ B^{(2)} \\ \cdot \\ B^{(N)} \\ C^{(1)} \\ C^{(2)} \\ \cdot \\ C^{(N)} \\ D^{(1)} \\ D^{(2)} \\ \cdot \\ D^{(N)} \\ F^{(1)} \\ \cdot \\ F^{(N-1)} \\ \cdot \\ F^{(N)} \end{pmatrix} = \begin{pmatrix} -P_{in} \\ -P_{out} \\ \cdot \\ 0 \\ 0 \\ 0 \\ \cdot \\ 0 \\ 0 \\ 0 \\ \cdot \\ 0 \\ 0 \\ \cdot \\ T \\ P \end{pmatrix} \quad \text{(A75)}$$

where

$$M = \begin{pmatrix} M_{1,1} & M_{1,2} & \cdot & M_{1,N} & \cdots\cdots & M_{1,3N+1} & M_{1,3N+2} & \cdot & M_{1,4N} \\ M_{2,1} & M_{2,2} & \cdot & M_{2,N} & \cdots\cdots & M_{2,3N+1} & M_{2,3N+2} & \cdot & M_{2,4N} \\ \cdot & \cdot & \cdot & \cdot & \cdots\cdots & \cdot & \cdot & \cdot & \cdot \\ M_{N,1} & M_{N,2} & \cdot & M_{N,N} & \cdots\cdots & M_{N,3N+1} & M_{N,3N+2} & \cdot & M_{N,4N} \\ M_{N+1,1} & M_{N+1,2} & \cdot & M_{N+1,N} & \cdots\cdots & M_{N+1,3N+1} & M_{N+1,3N+2} & \cdot & M_{N+1,4N} \\ M_{N+2,1} & M_{N+2,2} & \cdot & M_{N+2,N} & \cdots\cdots & M_{N+2,3N+1} & M_{N+2,3N+2} & \cdot & M_{N+2,4N} \\ \cdot & \cdot & \cdot & \cdot & \cdots\cdots & \cdot & \cdot & \cdot & \cdot \\ M_{2N,1} & M_{2N,2} & \cdot & M_{2N,N} & \cdots\cdots & M_{2N,3N+1} & M_{2N,3N+2} & \cdot & M_{2N,4N} \\ \cdot & \cdot & \cdot & \cdot & \cdots\cdots & \cdot & \cdot & \cdot & \cdot \\ \cdot & \cdot & \cdot & \cdot & \cdots\cdots & \cdot & \cdot & \cdot & \cdot \\ \cdot & \cdot & \cdot & \cdot & \cdots\cdots & \cdot & \cdot & \cdot & \cdot \\ \cdot & \cdot & \cdot & \cdot & \cdots\cdots & \cdot & \cdot & \cdot & \cdot \\ \cdot & \cdot & \cdot & \cdot & \cdots\cdots & \cdot & \cdot & \cdot & \cdot \\ \cdot & \cdot & \cdot & \cdot & \cdots\cdots & \cdot & \cdot & \cdot & \cdot \\ \cdot & \cdot & \cdot & \cdot & \cdots\cdots & \cdot & \cdot & \cdot & \cdot \\ M_{4N,1} & M_{4N,2} & \cdot & M_{4N,N} & \cdots\cdots & M_{4N,3N+1} & M_{4N,3N+2} & \cdot & M_{4N,4N} \end{pmatrix} \quad \text{(A76)}$$

M is structured according to Table IV.

From Equation (A67), the condition for radial stress at the inner radius gives:

$$F^{(1)}h^{(1)} + B^{(1)}r_1^{\kappa_1-1} + C^{(1)}r_1^{-\kappa_1-1} + D^{(1)}G^{(1)}r_1 = -P_{\text{in}} \quad \text{(A77)}$$

leading to row 1 of M defined as

$$M_{1,1} = r_1^{\kappa_1-1} \quad \text{(A78)}$$

$$M_{1,N+1} = r_1^{-\kappa_1-1} \quad \text{(A79)}$$

$$M_{1,2N+1} = G^{(1)}r_1 \quad \text{(A80)}$$

$$M_{1,3N+1} = h^{(1)} \quad \text{(A81)}$$

and from Equation (A68) the condition for radial stress at the outer radius gives:

$$F^{(N)}h^{(N)} + B^{(N)}r_{N+1}^{\kappa_N-1} + C^{(N)}r_{N+1}^{-\kappa_N-1} + D^{(N)}G^{(N)}r_{N+1} = -P_{\text{out}} \quad \text{(A82)}$$

leading to row 2

$$M_{2,N} = r_{N+1}^{\kappa_N-1} \quad \text{(A83)}$$

$$M_{2,2N} = r_{N+1}^{-\kappa_N-1} \quad \text{(A84)}$$

$$M_{2,3N} = G^{(N)}r_{N+1} \quad \text{(A85)}$$

$$M_{2,3N+1} = h^{(N)} \quad \text{(A86)}$$

From Equation (A69), for $j = 1$ to $N-1$, the condition for radial stress at contacting surfaces gives:

$$F(h^{(j+1)} - h^{(j)}) + B^{(j+1)}r_{j+1}^{\kappa_{j+1}-1} - B^{(j)}r_{j+1}^{\kappa_j-1} + C^{(j+1)}r_{j+1}^{-\kappa_{j+1}-1} - C^{(j)}r_{j+1}^{-\kappa_j-1} + r_{j+1}(D^{(j+1)}G^{(j+1)} - D^{(j)}\mu_1^{(j)}) = 0 \quad \text{(A87)}$$

Rows 3 to $N+1$ are therefore

$$M_{j+2,j} = -r_{j+1}^{\kappa_j-1} \quad \text{(A88)}$$

$$M_{j+2,j+1} = r_{j+1}^{\kappa_{j+1}-1} \quad \text{(A89)}$$

$$M_{j+2,N+j} = -r_{j+1}^{-\kappa_j-1} \quad \text{(A90)}$$

$$M_{j+2,N+j+1} = r_{j+1}^{-\kappa_{j+1}-1} \quad \text{(A91)}$$

$$M_{j+2,2N+j} = -r_{j+1}\mu_1^{(j)} \quad \text{(A92)}$$

$$M_{j+2,2N+j+1} = r_{j+1}\mu_1^{(j+1)} \quad \text{(A93)}$$

$$M_{j+2,3N+j} = -h^{(j)} \quad \text{(A94)}$$

$$M_{j+2,3N+j+1} = h^{(j+1)} \quad \text{(A95)}$$

from Equation (A70), for $j = 1$ to $N-1$ the condition for radial displacement at contacting surfaces gives:

$$(F^{(j+1)}[\eta_1^{(j+1)}]_2 - F^{(j)}[\eta_1^{(j)}]_2)r_{j+1} + B^{(j+1)}[\eta_2^{(j+1)}]_2 r_{j+1}^{\kappa_{j+1}} - B^{(j)}[\eta_2^{(j)}]_2 r_{j+1}^{\kappa_j} + C^{(j+1)}[\eta_3^{(j+1)}]_2 r_{j+1}^{-\kappa_j+1} - C^{(j)}[\eta_3^{(j)}]_2 r_{j+1}^{-\kappa_j} + (D^{(j+1)}[\eta_4^{(j+1)}]_2 - D^{(j)}[\eta_4^{(j)}]_2)r_{j+1}^2 = 0 \quad \text{(A96)}$$

rows $N+2$ to $2N-1$ are

$$M_{N+j+1,j} = -[\eta_2^{(j)}]_2 r_{j+1}^{\kappa_j} \quad \text{(A97)}$$

$$M_{N+j+1,j+1} = [\eta_2^{(j+1)}]_2 r_{j+1}^{\kappa_{j+1}} \quad \text{(A98)}$$

$$M_{N+j+1,N+j} = [\eta_3^{(j)}]_2 r_{j+1}^{-\kappa_j} \quad \text{(A99)}$$

$$M_{N+j+1,N+j+1} = -[\eta_3^{(j+1)}]_2 r_{j+1}^{-\kappa_{j+1}} \quad \text{(A100)}$$

TABLE IV Terms in the matrix

Rows	Conditions satisfied	Equation
1 to 2	Boundary conditions for radial stress at inner and outer surfaces	(A67) and (A68)
3 to $N+1$	Radial stress compatibility betweeen adjacent surfaces	(A69)
$N+2$ to $2N$	Radial displacement compatibility between adjacent surfaces	(A70)
$2N+1$ to $3N-1$	Shear stress compatibility between adjacent surfaces	(A71)
$3N$ to $4N-2$	Axial displacement compatibility between adjacent surfaces	(A72)
$4N-1$	Conditions for axial moment	(A74)
$4N$	Axial stresses summed across section give axial load	(A73)

$$M_{N+j+1,2N+j} = -[\eta_4^{(j)}]_2 r_{j+1}^2 \quad \text{(A101)}$$

$$M_{N+j+1,2N+j+1} = [\eta_4^{(j+1)}]_2 r_{j+1}^2 \quad \text{(A102)}$$

$$M_{N+j+1,3N+j} = -r_{j+1}[\eta_1^{(j)}]_2 \quad \text{(A103)}$$

$$M_{N+j+1,3N+j+1} = r_{j+1}[\eta_1^{(j+1)}]_2 \quad \text{(A104)}$$

from Equation (A71), for $j = 1$ to $N-1$ the condition for shear stress at contacting surfaces gives:

$$F^{(j+1)}\left(\frac{s_{34}^{(j+1)}}{\beta_{44}^{(j+1)}} + h^{(j+1)}g_1^{(j+1)}\right) - F^{(j)}\left(\frac{s_{34}^{(j)}}{\beta_{44}^{(j)}} - h^{(j)}g_1^{(j)}\right)$$
$$+ B^{(j+1)}g_{\kappa_j}^{(j+1)}r_{j+1}^{\kappa_{j+1}-1} - B^{(j)}g_{\kappa_j}^{(j)}r_{j+1}^{\kappa_j-1}$$
$$+ C^{(j+1)}g_{-\kappa_j}^{(j+1)}r_{j+1}^{-\kappa_{j+1}-1} - C^{(j)}g_{-\kappa_j}^{(j)}r_{j+1}^{-\kappa_j-1}$$
$$- D^{(j+1)}\mu_2^{(j+1)}r_{j+1} + D^{(j)}\mu_2^{(j)})r_{j+1} = 0 \quad \text{(A105)}$$

thus for rows $2N+1$ to $3N-1$

$$M_{2N+j,j} = -g_{\kappa_j}^{(j)}r_{j+1}^{\kappa_j-1} \quad \text{(A106)}$$

$$M_{2N+j,j+1} = g_{\kappa_{j+1}}^{(j)}r_{j+1}^{\kappa_{j+1}-1} \quad \text{(A107)}$$

$$M_{2N+j,N+j} = -g_{-\kappa_j}^{(j)}r_{j+1}^{-\kappa_j-1} \quad \text{(A108)}$$

$$M_{2N+j,N+j+1} = g_{-\kappa_{j+1}}^{(j)}r_{j+1}^{-\kappa_{j+1}-1} \quad \text{(A109)}$$

$$M_{2N+j,2N+j} = \mu_2^{(j)}r_{j+1} \quad \text{(A110)}$$

$$M_{2N+j,2N+j+1} = -\mu_2^{(j+1)}r_{j+1} \quad \text{(A111)}$$

$$M_{2N+j,3N+j} = -\frac{s_{34}^{(j)}}{\beta_{44}^{(j)}} - h^{(j)}g_1^{(j)} \quad \text{(A112)}$$

$$M_{2N+j,3N+j+1} = \frac{s_{34}^{(j+1)}}{\beta_{44}^{(j+1)}} + h^{(j+1)}g_1^{(j+1)} \quad \text{(A113)}$$

from Equation (A72), for $j = 1$ to $N-1$ the condition for axial load gives:

$$B^{(j+1)}[\eta_2^{(j+1)}]_3 r^{\kappa_j-1} - B^{(j)}[\eta_2^{(j)}]_3 r^{\kappa_j-1}$$
$$+ C^{(j+1)}[\eta_3^{(j+1)}]_3 r^{-\kappa_j-1} - C^{(j)}[\eta_3^{(j)}]_3 r^{-\kappa_j-1}$$
$$+ D^{(j+1)}[\eta_4^{(j+1)}]_3 r - D^{(j)}[\eta_4^{(j)}]_3 r$$
$$+ F^{(j+1)}[\eta_1^{(j+1)}]_3 - F^{(j)}[\eta_1^{(j)}]_3 = 0 \quad \text{(A114)}$$

rows $3N$ to $4N-2$ are

$$M_{3N+j-1,j} = -[\eta_2^{(j)}]_3 r_{j+1}^{\kappa_j} \quad \text{(A115)}$$

$$M_{3N+j-1,j+1} = [\eta_2^{(j+1)}]_3 r_{j+1}^{\kappa_{j+1}} \quad \text{(A116)}$$

$$M_{3N+j-1,N+j} = [\eta_3^{(j)}]_3 r_{j+1}^{-\kappa_j} \quad \text{(A117)}$$

$$M_{3N+j-1,N+j+1} = -[\eta_3^{(j+1)}]_3 r_{j+1}^{-\kappa_{j+1}} \quad \text{(A118)}$$

$$M_{3N+j-1,2N+j} = -[\eta_4^{(j)}]_3 r_{j+1}^2 \quad \text{(A119)}$$

$$M_{3N+j-1,2N+j+1} = [\eta_4^{(j+1)}]_3 r_{j+1}^2 \quad \text{(A120)}$$

$$M_{3N+j-1,3N+j} = -r_{j+1}[\eta_1^{(j)}]_3 \quad \text{(A121)}$$

$$M_{3N+j-1,3N+1} = r_{j+1}[\eta_1^{(j+1)}]_3 \quad \text{(A122)}$$

from Equation (A74), for $j = 1$ to N we have, for a fibre free to rotate;

$$\sum_{j=1}^{N}\left[\frac{F^{(j)}}{3}\left(\frac{s_{34}^{(j)}}{\beta_{44}^{(j)}} + h^{(j)}g_1^{(j)}\right)(r_{j+1}^3 - r_j^3)\right.$$
$$+ B^{(j)}g_{\kappa_j}^{(j)}\left(\frac{r_{j+1}^{\kappa_j+2} - r_j^{\kappa_j+2}}{\kappa_j+2}\right)$$
$$+ C^{(j)}g_{-\kappa_j}^{(j)}\left(\frac{r_{j+1}^{-\kappa_j+2} - r_j^{-\kappa_j+2}}{-\kappa_j+2}\right)$$
$$\left.- \frac{D^{(j)}\mu_2^{(j)}}{4}(r_{j+1}^4 - r_j^4)\right] = 0 \quad \text{(A123)}$$

the terms of row $4N-1$ are

$$M_{4N-1,j} = g_{\kappa_j}\left(\frac{r_{j+1}^{\kappa_j+2} - r_j^{\kappa_j+2}}{\kappa_j+2}\right) \quad \text{(A124)}$$

$$M_{4N-1,N+j} = g_{-\kappa_j}\left(\frac{r_{j+1}^{-\kappa_j+2} - r_j^{-\kappa_j+2}}{-\kappa_j+2}\right) \quad \text{(A125)}$$

$$M_{4N-1,2N+j} = -\frac{\mu_2^{(j)}}{4}(r_{j+1}^4 - r_j^4) \quad \text{(A126)}$$

$$M_{4N-1,3N+j} = \frac{1}{3}\left(\frac{s_{34}^{(j)}}{\beta_{44}^{(j)}} + h^{(j)}g_1^{(j)}\right)(r_{j+1}^3 - r_j^3) \quad \text{(A127)}$$

finally, the axial force balance from Equation (A73) gives for $j = 1$ to N

$$\sum_{j=1}^{N}\left[\frac{F^{(j)}}{2}\delta_1^{(j)}(r_{j+1}^2 - r_j^2) + B^{(j)}\delta_2^{(j)}\left(\frac{r_{j+1}^{\kappa_j+1} - r_j^{\kappa_j+1}}{\kappa_j+1}\right) - C^{(j)}\delta_3^{(j)}\left(\frac{r_{j+1}^{-\kappa_j+1} - r_j^{-\kappa_j+1}}{-\kappa_j+1}\right) + \frac{D^{(j)}}{3}\delta_4^{(j)}(r_{j+1}^3 - r_j^3)\right] = \frac{P}{2\pi} \quad \text{(A128)}$$

so row $4N$ is defined by

$$M_{4N,j} = \delta_2^{(j)}\frac{r_{j+1}^{\kappa_j+1} - r_j^{\kappa_j+1}}{\kappa_j+1} \quad \text{(A129)}$$

$$M_{4N,N+j} = \delta_3^{(j)}\frac{r_{j+1}^{-\kappa_j+1} - r_j^{-\kappa_j+1}}{-\kappa_j+1} \quad \text{(A130)}$$

$$M_{4N,2N+j} = \frac{1}{3}\delta_4^{(j)}(r_{j+1}^3 - r_j^3) \quad \text{(A131)}$$

$$M_{4N,3N+j} = \frac{1}{2}\delta_1^{(j)}(r_{j+1}^2 - r_j^2) \quad \text{(A132)}$$

Equation (A75) can now be solved to give the various constants A, B etc. Explicit expressions for stress, strain and displacements are therefore determined from Equations A47–A52 and the behaviour of the structure can be examined as a function of fibre winding angles and loading under axial load, torsion, and internal and external pressure.

References

1. D. ROBSON, J. HAGUE, G. NEWMAN, G. JERONIMIDIS and M. ANSELL, Survey of Natural Materials for use in Structural Composites as Reinforcement and Matrices. Technical report, The BioComposites Centre, University of Wales, Bangor, LL57 2UW, (1992).
2. A. SPENCER, *Compos. Sci. Technol.* **28** (1987) 173.
3. C. CAZENEUVE, P. JOGUET, J. C. MAILE and C. OYTANA, *Composites* **23** (1992) 415.
4. P. D. SODEN, R. KITCHING, P. C. TSE, Y. TSAVALAS and M. J. HINTON, *J. Mater. Sci.* **46** (1993) 363.
5. M. F. S. Al-KHALIL and P. D. SODEN, *Int. J. Mech. Sci.* **36** (1994) 49.
6. Y. MIKATA and M. TAYA, *J. Compos. Mat.* **19** (1985) 554.
7. C. M. WARWICK and T. W. CLYNE, *J. Mater. Sci.* **26** (1991) 3817.
8. M. W. K. ROSENOW, *Composites* **15** (1984) 144.
9. R. C. TANG, *Wood Fiber* **3** (1972) 210.
10. S. G. LEKHNITSKI, "Theory of Elasticity of an Anisotropic Body", (Mir Publishers, Moscow, 1981).
11. P. P. GILLIS, *Fib. Sci. Technol.* **2** (1970) 193.
12. I. M. WARD and A. P. WILCZYNSKI, *J. Mater. Sci.* **28** (1993) 1973.
13. W. C. ZHANG and K. E. EVANS, *Compos. Sci. Technol.* **29** (1988) 413.
14. P. A. WILCZYNSKI, *ibid.* **38** (1990) 327.
15. S. R. A. DYER, D. LORD, I. J. HUTCHINSON, I. M. WARD and R. A. DUCKETT, *J. Phys. D: Appl. Phys.* **25** (1992) 66.
16. S. K. BATRA, in "Handbook of Fibre Science and Technology: Fiber Chemistry", Vol. 4, edited by M. Lewin and E. M. Pearce (Marcel Dekker Inc., New York, 1995) p. 727.
17. M. HARRIS, "Harris's Handbook of Textile Fibres", (Gillette Research Laboratory, Bethesda, MA, 1954).
18. R. E. MARK, "Cell Wall Mechanics of Tracheids". (Yale University Press, New Haven, 1967).
19. R. Penrice (ed.) *Special Vehicle Engineer*, **8** (1995) 6.
20. F. L. MATTHEWS and R. D. RAWLINGS, "Composite materials: engineering and science", (Chapman and Hall, London, 1994).
21. J. LEMAITRE and J. L. CHABOUCHE, "Mechanics of Solid Materials", (Cambridge University Press, Cambridge, 1990).
22. S. P. TIMOSHENKO and J. N. GOODIER, "Theory of Elasticity", 3rd Edn. (McGraw-Hill, New York, 1970).

Received 19 April 1996
and accepted 28 January 1997